Neuron, Vol. 37, 775–786, March 6, 2003, Copyright ©2003 by Cell Press

The Presynaptic Active Zone Protein Bassoon Is Essential for Photoreceptor Ribbon Synapse Formation in the Retina

Oliver Dick,[1] Susanne tom Dieck,[1,2] Wilko Detlef Altrock,[2] Josef Ammermüller,[3] Reto Weiler,[3] Craig Curtis Garner,[4] Eckart Dieter Gundelfinger,[2] and Johann Helmut Brandstätter[1,*]

[1]Department of Neuroanatomy
Max Planck Institute for Brain Research
D-60528 Frankfurt/Main
[2]Leibniz Institute for Neurobiology
D-39118 Magdeburg
[3]AG Neurobiology
University of Oldenburg
D-26111 Oldenburg
Germany
[4]Department of Psychiatry and Behavioral Science
Stanford University
Palo Alto, California 94304

Summary

The photoreceptor ribbon synapse is a highly specialized glutamatergic synapse designed for the continuous flow of synaptic vesicles to the neurotransmitter release site. The molecular mechanisms underlying ribbon synapse formation are poorly understood. We have investigated the role of the presynaptic cytomatrix protein Bassoon, a major component of the photoreceptor ribbon, in a mouse retina deficient of functional Bassoon protein. Photoreceptor ribbons lacking Bassoon are not anchored to the presynaptic active zones. This results in an impaired photoreceptor synaptic transmission, an abnormal dendritic branching of neurons postsynaptic to photoreceptors, and the formation of ectopic synapses. These findings suggest a critical role of Bassoon in the formation and the function of photoreceptor ribbon synapses of the mammalian retina.

Introduction

Retinal photoreceptors transmit light signals over a dynamic range of several orders of magnitude in intensity. This level of performance is accomplished by a unique type of chemical synapse, the ribbon synapse (Dowling, 1987). The ribbon is a structurally and functionally specialized type of presynaptic active zone. It constitutes an electron-dense band of large surface area that extends from the site of transmitter release into the presynaptic cytoplasm and is covered by hundreds of synaptic vesicles (Rao-Mirotznik et al., 1995). At photoreceptor ribbon synapses, the release of the neurotransmitter glutamate onto the postsynaptic neurons occurs continuously and is modulated by small, graded changes in the presynaptic potential (DeVries and Baylor, 1993; Rieke and Schwartz, 1996). It is suggested that the ribbon accommodates a reservoir of readily releasable vesicles and is responsible for the fast and continuous vesicle supply for fusion at the release site. Therefore, the ribbon constitutes the precision machinery required for high-throughput focal exocytosis (for reviews see, von Gersdorff, 2001; Lenzi and von Gersdorff, 2001).

The synaptic ribbon is thought to be equivalent to the cytomatrix assembled at the active zone (CAZ) of conventional synapses (Garner et al., 2000) and is defined and organized by a scaffold of proteins. Two of these proteins are the very large and structurally related CAZ proteins Bassoon and Piccolo/Aczonin (Cases-Langhoff et al., 1996; tom Dieck et al., 1998; Wang et al., 1999; Fenster et al., 2000). They have been proposed to be involved in the structural and functional organization of the active zone (Garner et al., 2000; Dresbach et al., 2001). Bassoon and Piccolo are found at excitatory and inhibitory synapses in the brain (Richter et al., 1999; Fenster et al., 2000); they are among the earliest presynaptic proteins to appear at newly formed synapses (Vardinon-Friedman, 2000); and they are components of active zone precursor vesicles (Zhai et al., 2001). Mutant mice, deficient for functional Bassoon, suffer from epileptic seizures and have dysfunctional hippocampal synapses, although the ultrastructure of these synapses is indistinguishable from that of wild-type animals (Altrock et al., 2003 [this issue of *Neuron*]).

We have recently shown that Bassoon and Piccolo are integral components of photoreceptor ribbon synapses; at bipolar cell ribbon synapses, only Piccolo can be found (Brandstätter et al., 1999; Dick et al., 2001). We have also located Bassoon at the base of the photoreceptor synaptic ribbon, the site of transmitter release (Dick et al., 2001). To explore the functional role of Bassoon at photoreceptor ribbon synapses, we have examined, in this study, the retina of a mouse mutant lacking a functional Bassoon protein. We find that the absence of Bassoon prevents anchoring of the photoreceptor ribbon to the presynaptic active zone. This results in impaired photoreceptor synaptic transmission, affects the dendritic differentiation of postsynaptic neurons, and causes the formation of ectopic synapses. We propose that Bassoon serves a critical role in the formation and function of the photoreceptor ribbon synapse.

Results

Retinal Anatomy Is Normal in Homozygous *Bsn* Mutant Mice

As reported in an accompanying paper (Altrock et al., 2003), *Bsn* mutant mice express a residual 180 kDa protein (BsnΔEx4/5), which includes N-terminal and C-terminal regions of Bassoon, but lacks the central part of the protein encoded by exons 4 and 5 of the *Bsn* gene. As Bassoon is highly expressed in the rodent retina, we have first analyzed the retinal anatomy of homozygous *Bsn* mutant mice. In vertical sections of wild-type (wt) mouse retina, the Sap7f antiserum, recognizing the central part of Bassoon (tom Dieck et al., 1998), produces strong punctate labeling in the two syn-

*Correspondence: brandstaett@mpih-frankfurt.mpg.de

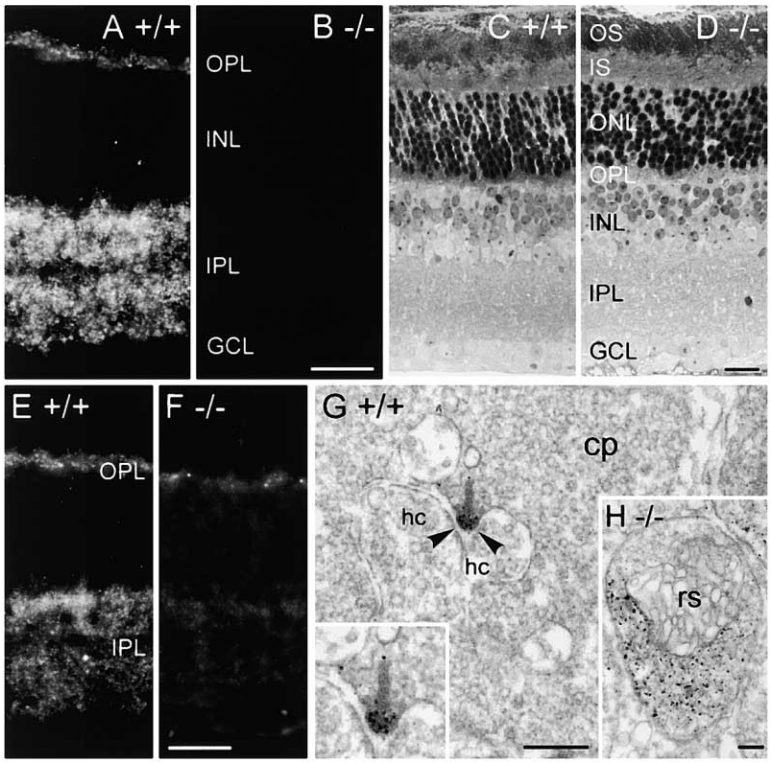

Figure 1. Comparison of Retinal Anatomy in Wild-Type (+/+) and Homozygous *Bsn* Mutant (−/−) Mice

(A and B) Vertical sections through +/+ and −/− retinae stained with the anti-Bassoon mab Sap7f. Whereas Sap7f strongly labels synaptic sites in the two synaptic layers of the +/+ retina, the OPL and the IPL, staining is absent in the −/− retina.

(C and D) A comparison of Toluidine blue-stained vertical semithin sections of +/+ (C) and −/− (D) retinae shows no effect of the *Bsn* mutation on the morphological appearance of the retina.

(E) The N-terminal anti-Bassoon pab BSN6.3 also labels synapses in the OPL and the IPL in the +/+ retina.

(F) In the −/− retina, weak and diffuse BSN6.3 immunoreactivity is still present in the IPL, and clusters of stronger BSN6.3 immunoreactivity in the OPL.

(G) Electron micrograph showing the localization of BSN6.3 immunoreactivity at the ribbon synaptic complex of a cone photoreceptor terminal (cp, cone pedicle) in the +/+ retina. The ribbon faces two postsynaptic horizontal cell processes (hc), and BSN6.3 immunoreactivity is concentrated at the base of the synaptic ribbon, the active zone of the synapse (arrowheads). This is best seen in the high-power view of the synapse (inset).

(H) Electron micrograph of a rod photoreceptor terminal (rs, rod spherule) in the −/− retina. No ribbon synaptic complex is present, and BSN6.3 immunoreactivity is diffusely distributed throughout the terminal. OS, outer segments; IS, inner segments; ONL, outer nuclear layer; OPL, outer plexiform layer; INL, inner nuclear layer; IPL, inner plexiform layer; GCL, ganglion cell layer. Scale bars, 20 μm (B, D, and F) and 0.2 μm (G and H).

aptic layers of the retina, the outer plexiform layer (OPL), and the inner plexiform layer (IPL) (Figure 1A). The immunofluorescent puncta represent presynaptic localization of Bassoon at the glutamatergic photoreceptor ribbon synapses in the OPL, and at conventional GABAergic and glycinergic synapses in the IPL (Brandstätter et al., 1999; Dick et al., 2001). In the *Bsn* mutant retina, the Sap7f epitope has disappeared completely (Figure 1B), whereas the overall structure of the retina with respect to thickness and lamination, three nuclear layers and two plexiform layers, is comparable to the wt retina (Figures 1C and 1D).

The antiserum BSN6.3, which is directed against the N-terminal region of Bassoon and recognizes both wt and mutant Bassoon protein (Altrock et al., 2003), produces a staining pattern similar to that of Sap7f in wt retina (Figure 1E). In the retina of homozygous *Bsn* mutant mice, BSN6.3 immunoreactivity is still detectable, but it is much weaker and more diffuse than in the wt retina (Figure 1F).

In a further analysis, we examined the ultrastructural distribution of wt Bassoon and BsnΔEx4/5 in photoreceptor terminals by preembedding immunocytochemistry and electron microscopy using the antiserum BSN6.3. In the wt retina, BSN6.3 immunoreactivity, like Sap7f immunoreactivity (Dick et al., 2001), was concentrated at the base of the photoreceptor synaptic ribbons, the site of glutamate release (Figure 1G). In the *Bsn* mutant retina, BSN6.3 immunoreactivity was diffusely distributed throughout the photoreceptor synaptic terminals (Figure 1H). This finding is similar to that reported by Altrock et al. (2003) who showed that the association of BsnΔEx4/5 with the cytomatrix at the active zone of synapses is severely impaired.

Absence of Photoreceptor Ribbon Synapses and Freely Floating Ribbons in the Retina of Homozygous *Bsn* Mutant Mice

Examining the distribution of BSN6.3 immunoreactivity in photoreceptor terminals of *Bsn* mutant retina, we noticed an absence of ribbon synapses. To further investigate this finding, we analyzed the photoreceptor terminals of mutant and wt retina qualitatively and quantitatively. We used single ultrathin sections and randomly photographed several hundred rod terminals from adult (4 months old) wt and *Bsn* mutant retinae. For the quantitative analysis, we focused on rod photoreceptors, as they make up 99% of the photoreceptors in the mouse retina.

The appearance of the ribbon synaptic complexes of rod and cone photoreceptors in the adult mutant retina differed significantly from those in the wt retina. Examples are shown in Figure 2, and quantitative data are summarized in Table 1. A normal rod synaptic terminal contains a single ribbon synaptic site, where glutamate is released onto the postsynaptic elements, horizontal cell processes, and rod bipolar cell dendrites. The postsynaptic elements invaginate into the rod terminal and form a triadic or tetradic configuration adjacent to the ribbon site (Figure 2A) (Rao-Mirotznik et al., 1995; Brandstätter and Hack, 2001).

In the adult *Bsn* mutant retina, only 17% of of rod

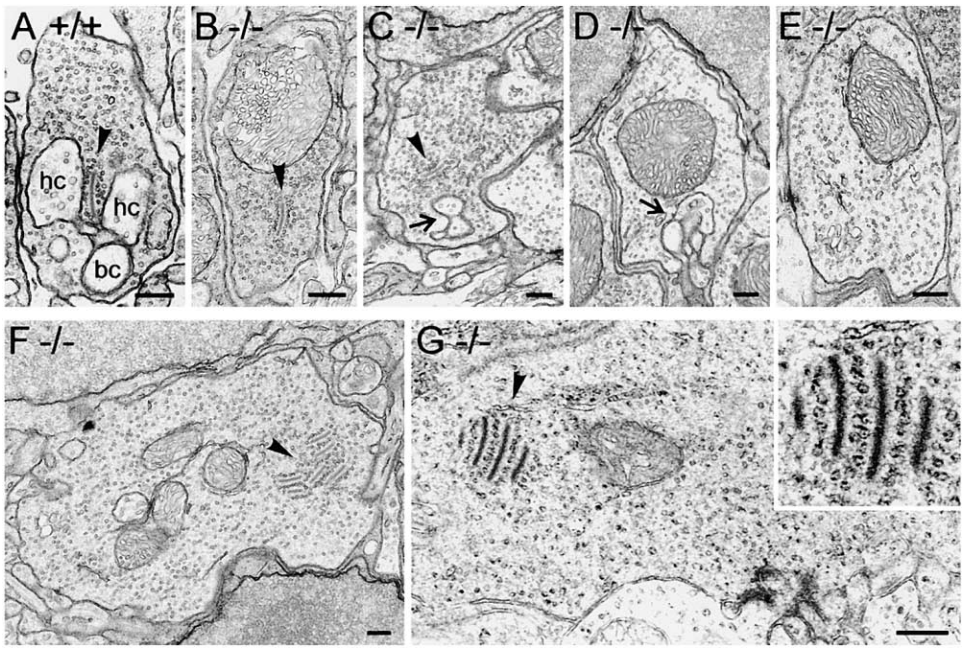

Figure 2. The Ultrastructural Appearance of the Photoreceptor Ribbon Synaptic Complex in the Homozygous *Bsn* Mutant (−/−) Retina

(A) Electron micrograph of a rod terminal and the triadic photoreceptor ribbon synaptic complex in wild-type (+/+) retina. The presynaptic ribbon (arrowhead) faces three postsynaptic elements, two horizontal cell processes (hc), and a rod bipolar cell dendrite (bc).

(B–E) Electron micrographs showing different examples of rod terminals and the ultrastructural appearance of the ribbon synaptic complex in the −/− retina: (B) terminal with a free-floating ribbon (arrowhead) and no postsynaptic elements, (C) terminal with free-floating ribbon (arrowhead) and postsynaptic elements (arrow), (D) terminal with postsynaptic elements (arrow) and no presynaptic ribbon, and (E) empty terminal.

(F and G) Cone photoreceptor synaptic terminals in the −/− retina. The free-floating presynaptic ribbons are aggregated in "ribbon fields" (arrowhead). Synaptic vesicles line the free ribbons, as seen in the high-power view of a ribbon field (inset, [G]). Scale bars, 0.3 μm.

terminals contained synaptic ribbons (56% in wt retina), and normal rod ribbon synapses were seen in less than 1% of the terminals (37% in wt retina) (Figure 2A; Table 1). Most of the ribbons in the mutant retina were not docked at the synaptic site but floated freely in the cytoplasm (Figures 2B and 2C). A similar number of rod terminals, in mutant and wt retinae (24%–28%), showed tight bundles of postsynaptic invaginating elements but no presynaptic ribbons (Figure 2D; Table 1). The proportion of empty rod terminals—terminals without presynaptic ribbons and postsynaptic invaginating elements—was 56% and 20% in mutant and wt retinae, respectively (Figure 2E; Table 1).

Free-floating ribbons were also present in the cone photoreceptor synaptic terminals (Figures 2F and 2G). A cone terminal contains several ribbon sites where glutamatergic signals are transmitted onto the processes of horizontal cells and the dendrites of various types of cone bipolar cells (Boycott and Wässle, 1999). In the cone terminals of adult mutant retinae, the free-floating ribbons were predominantly found arranged in aggregates, forming stacks of several ribbons with synaptic vesicles lining them (Figures 2F and 2G). Furthermore, fewer postsynaptic elements invaginated into the cone terminals in mutant as compared to wt terminals. In summary, the qualitative and quantitative data demonstrate that in the adult homozygous *Bsn* mutant retina, most of the photoreceptor ribbon synaptic complexes were absent.

Serial section reconstruction of photoreceptor synapses of *Bsn* mutant retina confirms that the freely floating ribbons are not attached to membrane (Figures 3A–3J). The bipolar cell ribbon synapses in the IPL, which only contain Piccolo but lack Bassoon (Brandstätter et al., 1999), can serve as an internal control for the photoreceptor synaptic phenotype in the mutant retina.

Table 1. Quantification of the Ultrastructural Appearance of the Rod Ribbon Synapse in Retinae of Adult Wild-Type (+/+) and Homozygous *Bsn* Mutant (−/−) Mice

Parameter	+/+ Σ 651 Rod Terminals	−/− Σ 522 Rod Terminals
Σ rod terminals + synaptic ribbons	363 (56%)	87 (17%)
Rod terminals + attached ribbons	243 (37%)	4 (<1%)
Rod terminals + free ribbons	120 (18%)	83 (16%)
Rod terminals + postsynaptic elements	156 (24%)	145 (28%)
Empty rod terminals	132 (20%)	290 (56%)

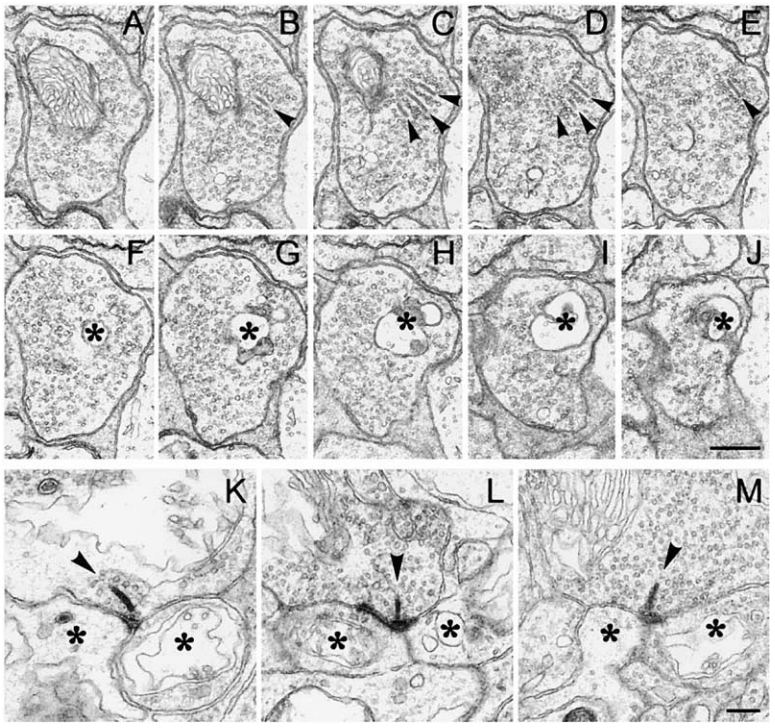

Figure 3. Free Photoreceptor and Attached Bipolar Cell Ribbons in the Homozygous *Bsn* Mutant (−/−) Retina

(A–J) Electron micrographs showing every second section of a series of ultrathin sections taken through a rod terminal in the −/− retina. Throughout the series, the freely floating ribbons (arrowheads) never attach to the presynaptic membrane or to any other membrane in the terminal.

(K–M) Bipolar cell synapses in the −/− retina. The ribbon (arrowhead) is attached to the presynaptic membrane. Postsynaptic elements are marked by asterisks. Scale bars, 0.5 μm (A–J) and 0.2 μm (K–M).

Consistent with this finding, the loss of Bassoon in the mutant retina has no effect on the integrity and the assembly of bipolar cell ribbon synapses (Figures 3K–3M).

Photoreceptor Ribbon Synapses in the Homozygous *Bsn* Mutant Retina Do Not Form during Postnatal Development

To address the question as to whether the observed adult synaptic phenotype in the *Bsn* mutant retina is a developmental or a degenerative phenotype, we studied the postnatal development of the photoreceptor ribbon synapse.

The mouse retina matures postnatally. At postnatal day 0 (P0) (Figure 4A), Bassoon immunoreactivity is already present in neurons and their processes stratifying in the IPL, followed by Bassoon expression in the OPL at around P4 (Figure 4A). Hand in hand with neuronal differentiation and the maturation of chemical synapses, the staining for Bassoon increased in the two plexiform layers. In the OPL, Bassoon expression reached its mature levels at around 2 weeks postnatally (Figure 4A; P15), while in the IPL it continued to increase up to the third to fourth postnatal week (Figure 4A; P21). During the first 2 weeks of postnatal development, Bassoon staining changed from a diffuse to a punctate appearance, and from a homogeneous distribution pattern in the IPL to a stratified pattern with bands of higher and lower staining intensity (Figure 4A; P0–P15).

In the wt mouse retina, the first triadic photoreceptor ribbon synapses are found during the second postnatal week (Blanks et al., 1974). Therefore, we have chosen the postnatal stages P10, P14, and 5 weeks for the developmental study and examined with electron microscopy several hundred photoreceptor terminals from wt and mutant retinae at each stage. The principal results are documented in Figures 4B and 4C (see also Supplementary Table S1 at http://www.neuron.org/cgi/content/full/37/5/775/DC1). At each stage, we found many more photoreceptor terminals containing ribbons in the wt retinae (50%–60%) than in the *Bsn* mutant retinae (20%–30%) (Figure 4B). The size of the terminals did not vary between wt and mutant retinae. In wt retinae, 40%–80% of the photoreceptor ribbons were attached to the presynaptic membrane, and 20%–60% floated freely in the cytoplasm of the terminals at the different postnatal stages (Figure 4C). This was significantly different from the *Bsn* mutant retinae, where only 1%–5% of photoreceptor ribbons were attached at the synaptic sites (Figure 4C). It is important to note that between P10 and 5 weeks, the number of attached ribbons in the wt retina significantly increased (40% → 80%), while, in turn, the number of free ribbons decreased (60% → 20%). This documents the ongoing formation of photoreceptor ribbon synapses in wt retinae during this developmental period, which did not take place in the *Bsn* mutant retinae (Figure 4C). These results indicate that the synaptic phenotype in the adult homozygous *Bsn* mutant retina is due to a developmental failure and not to degeneration.

Modifications in Dendritic Branching Patterns and Ectopic Ribbon Sites in the Homozygous *Bsn* Mutant Retina

The postsynaptic elements at photoreceptor ribbon synapses are rod bipolar, cone bipolar, and horizontal cells. To analyze possible morphological modifications of these neurons in the adult *Bsn* mutant retina, we performed a series of immunocytochemical experiments and confocal laser-scanning microscopy.

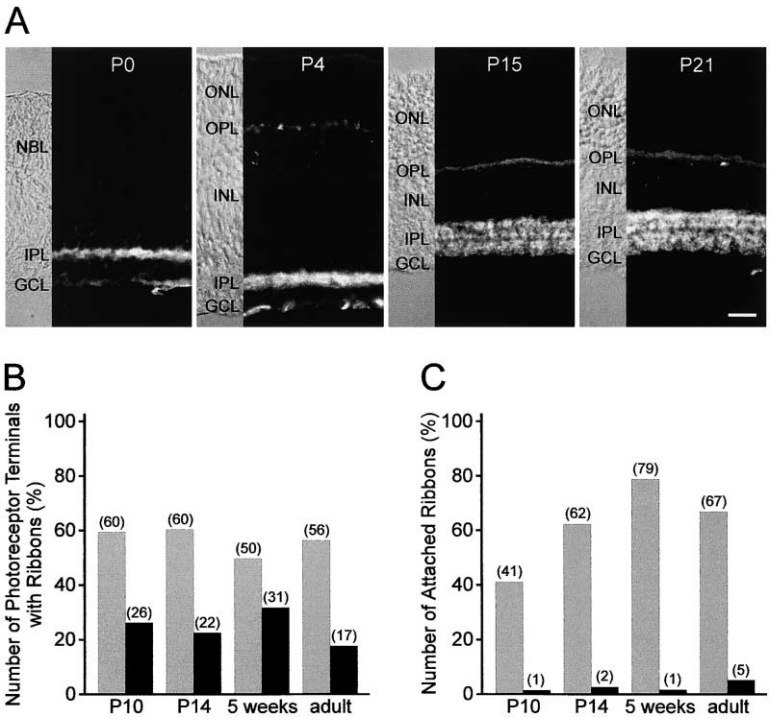

Figure 4. Postnatal Expression of Bassoon Immunoreactivity and Quantification of Photoreceptor Ribbon Synapse Development in Wild-Type and Homozygous *Bsn* Mutant Retinae

(A) Vertical sections through wild-type mouse retinae of different postnatal developmental stages, P0, P4, P15, and P21, stained with the anti-Bassoon mab Sap7f. Nomarski micrographs show the retinal layers. At the day of birth (P0), Bassoon immunoreactivity is already present in the IPL. In the developing OPL, first Bassoon immunoreactivity is found at around P4. The staining intensity in the OPL gradually increases up to the end of the second postnatal week, while in the IPL it continues to increase up to the fourth postnatal week. During the first 2 postnatal weeks the typical punctate synaptic labeling for Bassoon develops, and the homogeneous distribution of Bassoon immunofluorescence in the IPL changes to a stratified pattern. 3 weeks postnatally, the expression of Bassoon has reached the adult labeling pattern.

(B) In the wild-type retinae (gray bars) significantly more photoreceptor terminals contain synaptic ribbons than in the homozygous *Bsn* mutant retinae (black bars) at all developmental stages examined.

(C) In the homozygous *Bsn* mutant retinae (black bars), a negligible number of ribbons is found attached to the presynaptic membrane, compared to the wild-type retinae (gray bars) at all developmental stages examined. Numbers in brackets indicate percentage of photoreceptor terminals with ribbons (B) and percentage of attached ribbons (C). Abbreviations are as in Figure 1. NBL, neuroblast layer. Scale bar, 20 μm.

Horizontal Cells

In the mouse retina, a single type of horizontal cell exists, the B-type horizontal cell (Peichl and González-Soriano, 1994). The dendrites of the B-type cell contact cone terminals, and the axon terminal system of the B-type cell contact rod terminals. To assess the appearance of horizontal cells, we used an antiserum against the calcium binding protein Calbindin—a marker for these cells (Haverkamp and Wässle, 2000). In the OPL of wt retina, the horizontal cell processes form a regular and dense plexus (Figure 5A), whereas in the mutant retina, horizontal cell morphology was dramatically altered. Most strikingly, horizontal cell processes extended far beyond the OPL into the outer nuclear layer (ONL; Figure 5B). In double-labeling experiments (Figure 5C), we stained horizontal cells with Calbindin antibodies and photoreceptor synaptic ribbons with an antibody against the motor protein kinesin (Muresan et al., 1999). In the wt retina, presynaptic photoreceptor ribbons (red) face postsynaptic horizontal cell processes (green) (Figure 5C). Surprisingly, in the *Bsn* mutant retina, the horizontal cell processes also colocalized with photoreceptor ribbons at their ectopic position in the ONL (Figure 5D). Ectopic localization of photoreceptor ribbon synapses in the ONL was never observed in the wt retina.

Rod Bipolar Cells

An antibody against PKCα served as a marker to stain rod bipolar cells (Haverkamp and Wässle, 2000). In the wt retina, dendrites of these cells end in the OPL where they invaginate into the terminals of rod photoreceptors (Figure 5E). In the *Bsn* mutant retina, the rod bipolar cell dendritic plexus was significantly altered (Figure 5F). There appeared to be fewer, less densely arranged dendrites, and most strikingly, the dendrites extended far into the ONL (Figure 5F). In double-labeling experiments, we stained rod bipolar cells with PKCα (green) and the metabotropic glutamate receptor 6 (mGluR6; red in Figures 5G and 5H), which is the the most prominent postsynaptic glutamate receptor in the dendritic tips of rod bipolar cell (Nomura et al., 1994; Masu et al., 1995). In the mutant retina, rod bipolar cells expressed mGluR6 ectopically in dendrites localized in the ONL (Figure 5H), and mGluR6 clusters colocalized with photoreceptor ribbons (data not shown). mGluR6 was also expressed in rod bipolar cell dendrites stratifying in the OPL (Figure 5H).

OFF-Cone Bipolar Cells

To stain OFF-cone bipolar cells, the postsynaptic elements at flat, basal synapses of cone terminals (Kolb and Nelson, 1995), we used an antiserum against the neurokinin-3 receptor (Casini et al., 2000). A comparison between wt (Figure 5I) and *Bsn* mutant retina (Figure 5J) showed no obvious differences in the dendritic stratification pattern of the OFF-cone bipolar cells. The dendrites stratified within the OPL and did not grow into the ONL in the *Bsn* mutant retina (Figures 5I and 5J).

ON-Cone Bipolar Cells

ON-cone bipolar cells are postsynaptic at the invaginating ribbon synapses of cone terminals (Kolb and Nelson, 1995). There is no marker available that exclusively labels ON-cone bipolar cells. An antiserum against $G_o\alpha$ stains ON-cone bipolar cells and rod bipolar cells (Figure 5K) (Haverkamp and Wässle, 2000). In double-labeling experiments we combined the antibodies against $G_o\alpha$ and the rod bipolar cell marker PKCα. We found that only double-labeled bipolar cells, i.e., rod bipolar cells,

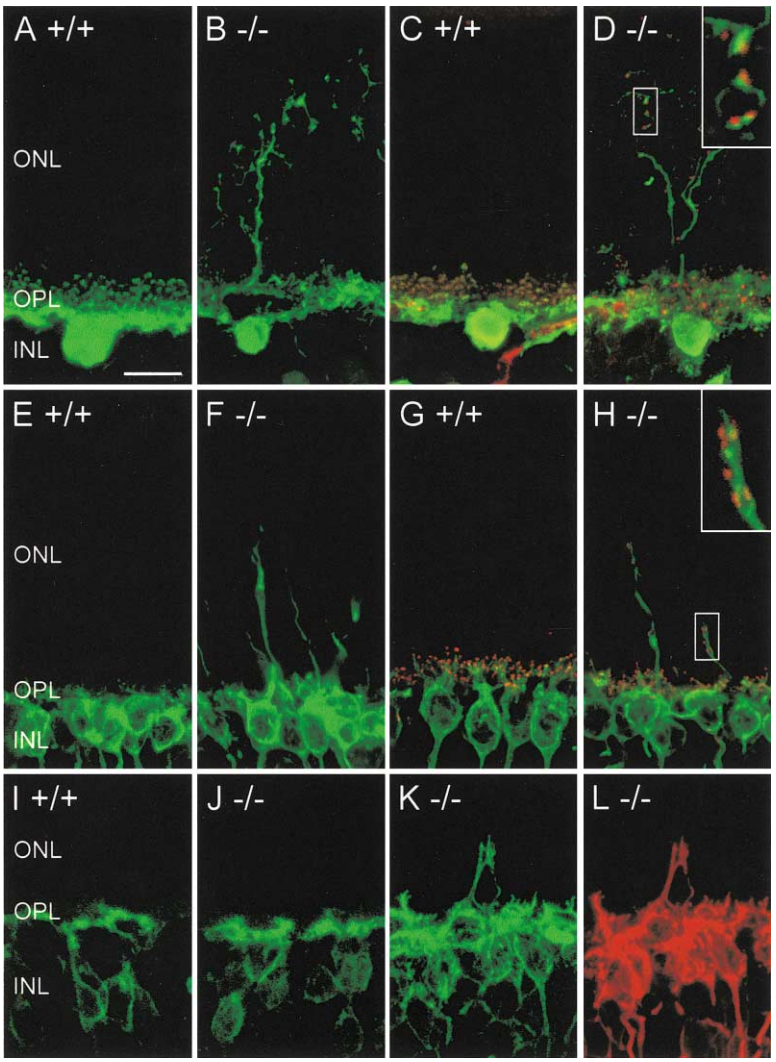

Figure 5. Cellular Changes in the Homozygous *Bsn* Mutant (−/−) Retina

(A–L) Confocal micrographs of vertical sections through wild-type (+/+) and −/− retinae stained with antibodies labeling distinct populations of retinal neurons and synaptic sites. (A–D) Retinal sections single labeled for horizontal cells (A and B) and double labeled for horizontal cells and photoreceptor synaptic ribbons (C and D). Horizontal cell processes in the −/− retina grow into the ONL (B), which is not the case in the +/+ retina (A). The outgrowing horizontal cell processes (green) are in contact with presynaptic photoreceptor ribbons (red) (D). The inset in (D) shows a magnification of the selected area (box). (E–H) Retinal sections single-labeled for rod bipolar cells (E and F) and double-labeled for rod bipolar cells and mGluR6 (G and H). Rod bipolar cell dendrites in the −/− retina extend far out into the ONL (F), which is not the case in the +/+ retina (E). The rod bipolar dendrites in the ONL (green) express mGluR6 (red) (H). The inset in (H) shows a magnification of the selected area (box). (I and J) Retinal sections single-labeled for OFF-cone bipolar cells. The dendrites of the OFF-cone bipolar cells in the −/− retina (J) stratify within the OPL, like in the +/+ retina (I). (K and L) Single section of −/− retina double labeled for ON-cone and rod bipolar cells (K) and for rod bipolar cells only (L). The ON-cone bipolar cells stratify within the OPL, and only the rod bipolar cell dendrites grow into the ONL (K). Abbreviations are as in Figure 1. Scale bar, 10 μm.

extended their dendrites into the ONL in the *Bsn* mutant retina (Figures 5K and 5L). This suggests that, like OFF-cone bipolar cells, ON-cone bipolar cells do not grow their dendrites into the ONL.

Ectopic ribbon sites were further examined for the presence of the vesicular glutamate transporter 1 (VGLUT1; red immunofluorescence), an essential component of glutamatergic synapses (Takamori et al., 2000). Postsynaptic elements, rod bipolar cell dendrites and horizontal cell processes, were visualized with antibodies against PKCα and Calbindin, respectively (green immunofluorescence). In the wt retina, VGLUT1 immunoreactivity was restricted to the photoreceptor terminals in the OPL (Figures 6A and 6B). In the mutant retina, in contrast, many photoreceptors localized VGLUT1 in the ONL, at sites where they were contacted by arborizing processes from rod bipolar and horizontal cells (Figures 6C and 6D).

Electron microscopy corroborated the light microscopical findings. Here, we found ectopic ribbons and postsynaptic processes of putative horizontal and rod bipolar cells in the ONL of the *Bsn* mutant retina. Importantly, only rod photoreceptors expressed ectopic ribbon synapses. To our surprise, the ribbons were attached to the presynaptic membrane and, sometimes, coated vesicles were present suggesting exo-/endocytotic activity at these ectopic synapses (Figures 6E and 6F).

Impaired Photoreceptor Synaptic Transmission in the Homozygous *Bsn* Mutant Retina

Finally, we analyzed the *Bsn* mutant retina at the functional level by performing electroretinographic (ERG) recordings. ERG responses to a short light flash are divided into three major components, the a-, b-, and c-waves (Dowling, 1987; Steinberg et al., 1991). Each wave represents a mass response generated by complex interactions in the retina. Although the exact origin and generation are still partially elusive, it has become clear that the a-wave mainly originates in photoreceptor cells and the b-wave principally arises from second-order cells, while the c-wave reflects activity of Müller cells and the pigment epithelium (Steinberg et al., 1991; Masu et al., 1995).

It was still possible to record a scotopic ERG from *Bsn* mutant mice with discernable a-, b-, and c-waves. The three components, however, were differentially af-

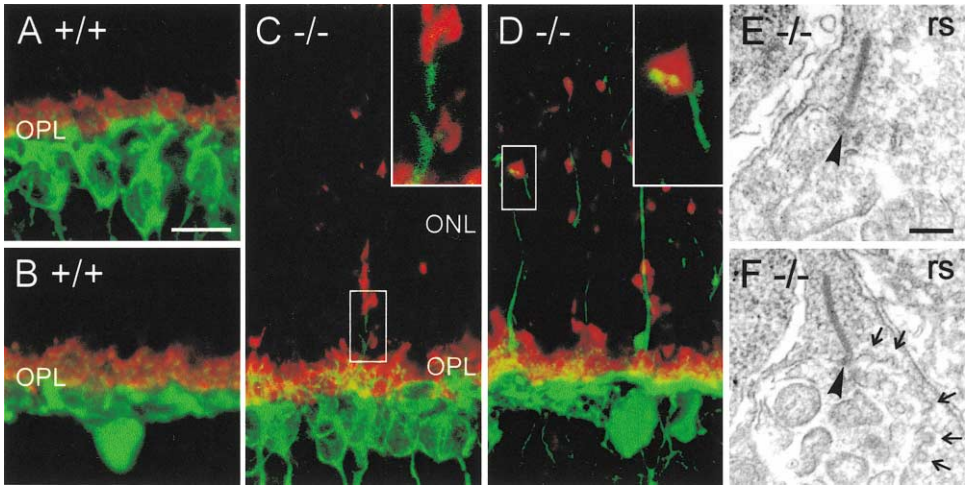

Figure 6. Ectopic Ribbon Synapses in the ONL of the Homozygous *Bsn* Mutant (−/−) Retina

(A–D) Confocal micrographs of vertical sections through wild-type (+/+) and −/− retinae double labeled for VGLUT1 (red) and rod bipolar or horizontal cells (green). (A and B) In the +/+ retina, VGLUT1 is expressed in the photoreceptor terminals in the OPL. The presynaptic terminals are contacted by the postsynaptic dendrites and processes of rod bipolar (A) and of horizontal (B) cells, respectively. (C and D) In the −/− retina, photoreceptors express VGLUT1 also in an ectopic localization in the ONL. Here, the sprouting dendrites and processes of rod bipolar (C) and of horizontal (D) cells, respectively, contact the photoreceptors. The insets in (C) and in (D) show a higher magnification of the selected areas (box).

(E and F) Electron micrographs of ectopic ribbon synaptic sites. The ribbon is attached to the presynaptic membrane (arrowhead) and faces postsynaptic elements. The arrows in (F) mark coated vesicles, indicating endo-exocytotic activity at ectopic ribbon synapses. Abbreviations are as in Figure 1. Scale bars, 10 μm (A) and 0.2 μm (E).

fected and showed distortions (Figures 7A and 7B). The c-wave amplitudes were decreased in mutant mice but were not studied further since they arise from nonneuronal elements. The a- and the b-waves were analyzed quantitatively since they reflect neuronal activity. The a-wave amplitudes in mutant mice were similar to those of wt mice and showed the same light intensity dependence (Figure 7C). The amplitude of the b-wave, on the other hand, was smaller in mutant mice, and for intensities above 10 lux (lx), the difference drastically increased. In the mutant, b-wave amplitudes reached a maximum at about 2 lx and then declined to a somewhat lower level with increasing intensities. Oscillations of the b-wave could be discerned both in wt and mutant mice, but were of much lower frequency in mutant mice (Figure 7B). The implicit time (time-to-peak) versus intensity curves for the a-waves were identical in both types of animals (Figure 7D). The implicit times of the b-wave, on the other hand, were longer in *Bsn* mutant mice at intensities above approximately 10 lx, confirming that the b-wave developed slower in these mice.

Next, the cone pathway was studied by presenting light flashes on backgrounds of increasing intensities (Figures 7E–7G). Incremental threshold functions were measured by determining the intensity needed to reach a 20 μV threshold criterion response at the various background intensities. As under scotopic conditions, mainly b-wave amplitudes were reduced in *Bsn* mutant mice compared to wt (Figures 7E and 7F). The incremental threshold functions of the b-wave closely followed a Weber-Fechner relation ($\Delta_L/\Delta_{Lo} = k(L + L_o)^n$) in both wt and mutant mice (Figure 7G). The function for the mutant, however, significantly deviated from the one obtained from wt animals at background illuminances above approximately 0.1 lx. At these higher background illuminances, *Bsn* mutant mice had much higher incremental thresholds, and at backgrounds above 10 lx, our stimulus light was not sufficiently bright to elicit the criterion response at all. On the other hand, incremental threshold functions of the a-wave were statistically identical in mutant and wt mice. Taken together, the data from the ERG recordings show that transmission from photoreceptor ribbon synapses to postsynaptic bipolar cells is perturbed.

Discussion

Active zones of vertebrate synapses are highly organized structures designed for the regulated and site-specific release of neurotransmitter. While the proteins that comprise the cytoskeletal matrix assembled at active zones have been suggested to be central organizers that provide the structural scaffold to ensure rapid and efficient docking and fusion of synaptic vesicles (Garner et al., 2000; Dresbach et al., 2001), direct proof for this hypothesis is lacking. Our studies of central nervous system synapses have identified the presynaptic active zone proteins, Bassoon and Piccolo, as structural components of the active zone. Both belong to the same gene family and share numerous structurally related subdomains, indicating that they may perform related, possibly redundant, functions at active zones (Fenster et al., 2000). The functional characterization of Piccolo and Bassoon has been hampered inpart by the fact that they are generally found together at the active zones of both glutamatergic and GABAergic synapses (Richter et al., 1999). An exception is the ribbon synapse in the retina. Here, we have found that bipolar cell ribbon syn-

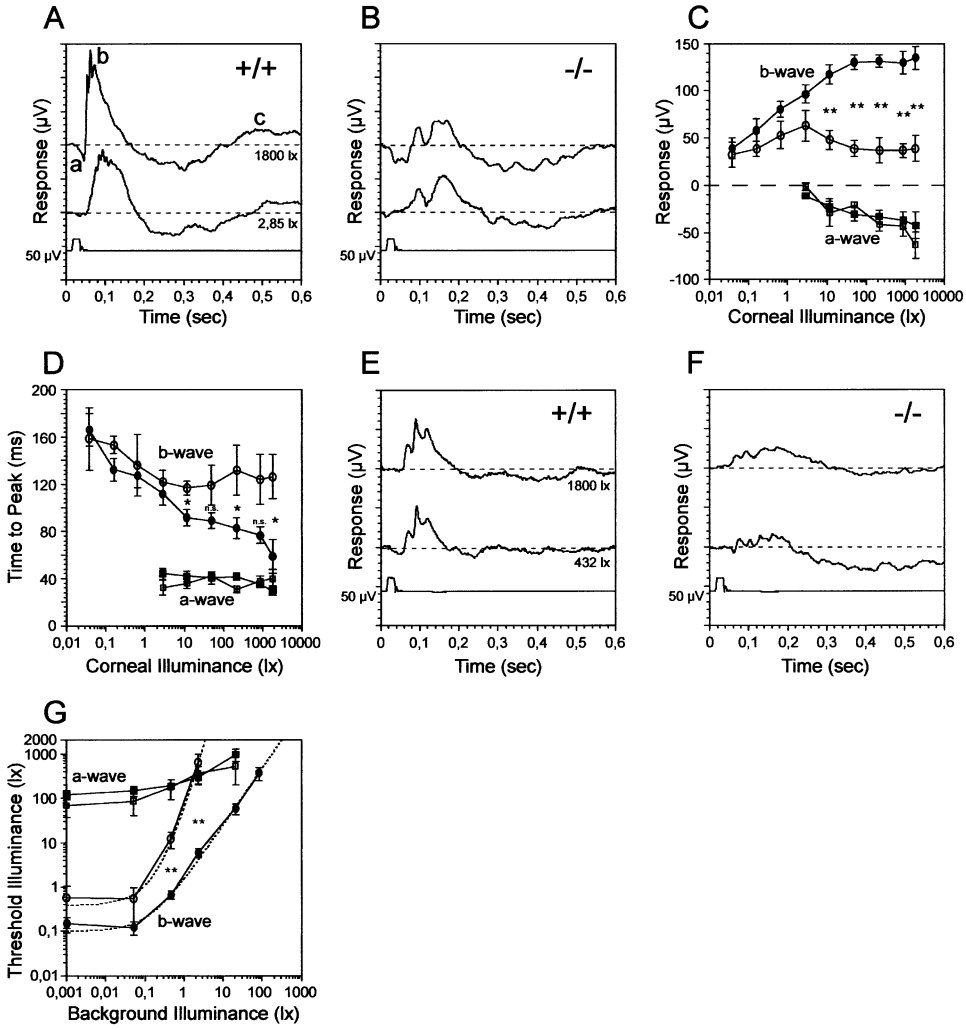

Figure 7. Scotopic and Photopic ERG Recordings and Increment Threshold Curves from Wild-Type (+/+) and Homozygous *Bsn* Mutant (−/−) Retinae

(A and B) Examples for scotopic responses of +/+ (A) and −/− mice (B) to 20 ms white light flashes of 1800 and 2.85 lx. −/− mice show decreased b- and c-wave amplitudes and slower b-wave oscillations than +/+ mice. a-wave amplitudes are similar. Amplitudes were measured with respect to the dark base level (dashed lines).

(C) Intensity-response curves for the a- (squares) and b- (circles) waves in −/− mice (open symbols) and +/+ mice (filled symbols). b-wave amplitudes are significantly smaller in −/− mice for intensities in excess of about 10 lx and even decreased with higher intensities. a-wave amplitudes are identical.

(D). Time-to-peak versus intensity curves of a-waves (squares) are identical in −/− (open symbols) and +/+ (filled symbols) mice. b-wave time-to-peak (circles) is longer in −/− mice for intensities in excess of 10 lx and saturates at about 120–140 ms.

(E and F) Examples for photopic responses of +/+ (E) and −/− mice (F) to 20 ms white light flashes of 1800 and 432 lx, superimposed upon a steady background of 2.85 lx.

(G) Increment threshold curves for a- (squares) and b- (circles) waves of −/− (open symbols) and +/+ (filled symbols) mice. Data points plot the mean ± SEM threshold illuminance for evoking a 20µV threshold response on a given steady background. a-wave incremental threshold functions do not differ. −/− mice show significantly increased thresholds for background intensities in excess of about 0.1 lx. Dotted lines indicate Weber-Fechner fits of the b-wave data points ($\Delta L/\Delta L_o = k(L - L_o)^n$; for −/− mice: $R^2 = 0.999$; $\Delta L_o = 0.4$ lx; $k = 70.2$; $n = 3.26$; $L_o = 0.27$ lx; for +/+ mice: $R^2 = 0.999$; $\Delta L_o = 0.095$ lx; $k = 13.6$; $n = 1.28$; $L_o = 0.14$ lx (ΔL, incremental threshold illuminance; ΔL_o, absolute threshold; L, background illuminance; L_o, "dark" light or Fechner's "Eigengrau;" k and n are constants). Data points plot the mean ± SEM ($n = 6$ for −/− mice and $n = 8$ for +/+ mice). *$p < 0.05$; **$p < 0.01$; Mann-Whitney U test; n.s. = not significant).

apses only contain Piccolo, while photoreceptor ribbon synapses contain both Piccolo and Bassoon (Brandstätter et al., 1999, Dick et al., 2001). To gain information on the role of Bassoon at photoreceptor ribbon synapses, we have examined the effects of the loss of Bassoon. Our results reveal that the integrity of photoreceptor ribbon synapses is gravely compromised, while the loss of a functional Bassoon protein has no effect on the assembly of bipolar cell ribbon synapses, consistent with the absence of Bassoon from this synapse (Brandstätter et al., 1999). These data strongly implicate the cytomatrix protein Bassoon in the formation and functionality of the photoreceptor ribbon synapse in the retina, and specifically in the attachment of the photore-

ceptor ribbon to the presynaptic active zone. The data are further proof that the molecular composition of photoreceptor and bipolar cell ribbons is different.

Bassoon Is Required for Anchoring of the Photoreceptor Ribbon to the Presynaptic Active Zone

Maturation of photoreceptor ribbon synapses in the mouse retina occurs stepwise: at around P4, the first anchored presynaptic ribbons appear at sites where postsynaptic horizontal cell processes contact photoreceptor terminals. This is followed by the invagination of the postsynaptic elements into the photoreceptor terminal and the formation of a triadic synaptic complex consisting of the presynaptic ribbon, two lateral horizontal cell processes, and a central bipolar cell dendrite between P10 and P14 (Blanks et al., 1974).

In the OPL of the *Bsn* mutant retinae, we found only a negligible number of ribbons attached to the presynaptic membrane. The absence of attached ribbons, throughout postnatal retinal development, demonstrates that Bassoon is required for the anchoring of the photoreceptor ribbon to the active zone during synaptogenesis.

At 5 postnatal weeks, the highest number of freely floating ribbons in mutant photoreceptor terminals was observed. Many of these ribbons appeared as small densities (O.D. and J.H.B., unpublished data). These "mini ribbons" are reminiscent of the small ribbon densities found in cone synaptic terminals of the zebrafish *no optokinetic response c* (*nrc*) mutant (Allwardt et al., 2001) and the small round precursor bodies found in developing rat photoreceptor terminals (Hermes et al., 1992; Vollrath and Spiwoks-Becker, 1996). The protein RIBEYE, a major component of the synaptic ribbon, is suggested to be the scaffold for building the ribbon structure in a modular way (Schmitz et al., 2000). It is possible that the small densities found in the photoreceptor terminals of the *Bsn* mutant retina are degradation products of larger ribbons that have disintegrated into smaller protein aggregates due to the absence of functional Bassoon.

In addition to Bassoon, the related presynaptic cytomatrix protein Piccolo is present at photoreceptor ribbon synapses (Dick et al., 2001). The results of this study demonstrate that Piccolo cannot compensate for the lack of full-length Bassoon at the photoreceptor ribbon synapse. This appears to be in contrast to conventional brain synapses, where Piccolo content is upregulated, and the ultrastructural appearance of synapses is unaltered as compared to wild-type (Altrock et al., 2003). Interestingly, the absence of full-length Bassoon does not preclude recruitment of Piccolo to the floating ribbon (O.D. and J.H.B., unpublished data). These observations indicate that despite their structural similarities, they perform distinction roles in the establishment of functional ribbons. For Bassoon, this appears to involve a physical link between ribbons and the plasma membrane—possibly via N-terminal acetylation, as it has a predicted myristoylation motif at the N terminus (T. Dresbach, C. Spilker, and E.D.G., unpublished data). However, N-myristoylation alone appears insufficient for efficient membrane association, as BsnΔEx4/5 can be easily extracted from membrane fractions (Altrock et al., 2003). Alternatively, the absence of functional Bassoon could cause inappropriate assembly of synaptic ribbons, which then cannot be anchored to the active zone. This assumption, however, cannot explain why ribbons can be anchored at ectopic synapses. The later observation rather suggests that there may be a timing problem. The lack of Bassoon may cause a delay in production of functional ribbons, and once they are available, signals for timely and spatially appropriate synapse formation have vanished.

The suggested function for photoreceptor ribbons is to continuously shuttle vesicles to the active zone for fusion and release of glutamate (Lenzi and von Gersdorff, 2001; von Gersdorff, 2001). Ribbons that are not attached to the active zone should result in failure of synaptic transmission. This is consistent with the ERG recordings from the *Bsn* mutant mouse. The a-wave of the ERG, representing rod and cone photocurrents, was not affected by the *Bsn* mutation. However, the b-wave, representing the massed response of the ON bipolar cells was significantly reduced in amplitude, and the implicit times were prolonged. The amplitude of the residual b-wave in the *Bsn* mutant mouse was not different between the scotopic and the photopic ERG, suggesting its origin is in the rod system of the retina.

The zebrafish *nrc* mutant displays a functional and morphological retinal phenotype similar to the homozygous *Bsn* mutant mouse (Allwardt et al., 2001). The candidate gene responsible for the mutation in the zebrafish is not known. Nonetheless, in contrast to the Bassoon mutation, *nrc* mutations mainly affect cone photoreceptors and their ribbon synapses. In the *nrc* mutant, postsynaptic elements, and here especially bipolar cell dendrites, fail to penetrate into the developing cone synaptic terminals, resulting in a failure to form ribbon synaptic complexes (Allwardt et al., 2001). In the *Bsn* mutant retina, the postsynaptic elements invaginate into the photoreceptor terminals, suggesting that in the mammalian retina the process of invagination does not require the presence of an anchored ribbon.

A block of bipolar cell dendrite insertion in the final stages of photoreceptor ribbon synapse formation is also discussed as a main reason for the disrupted synaptic connections between photoreceptors and second-order cells found in mice deficient of the laminin β2 chain (Libby et al., 1999). As the laminin β2 chain is expressed in the extracellular matrix of the OPL, the photoreceptor synaptic disruption in the β2 chain-deficient mice has a postsynaptic origin, different from the presynaptic origin in the *Bsn* mutant retina.

Abnormal photoreceptor terminals and synapses and a severely affected ERG have been also reported for the retina of a naturally occurring substrain of C57BL/10 mice (Ruether et al., 2000). The location of the gene defect is not known, but it is not likely to be Bassoon, as there are several distinct differences to the Bassoon mutation. In the naturally occurring mouse mutant, the number of photoreceptors is reduced, and rod photoreceptor terminals contain neither ribbons nor invaginations. In addition to the photoreceptor ribbon synapses, the bipolar cell ribbon synapses in the IPL are perturbed (in 3-month-old mice, ribbons were completely absent in the IPL) (Ruether et al., 2000). In the *Bsn* mutant retina, bipolar cell ribbon synapses were not affected. This is not surprising, as Bassoon is absent

from these synapses (Brandstätter et al., 1999). Instead, our data indicate that Piccolo is specifically associated with the bipolar cell ribbon synapse (Dick et al., 2001).

Ectopic Ribbon Synapses and Dendritic Modifications of Second-Order Neurons in the Homozygous *Bsn* Mutant Retina

Taken together, our morphological and physiological results suggest that the ectopic ribbon synapses in the ONL and the ribbon synapses which are still formed in the OPL in the absence of functional Bassoon are most likely functional. Morphologically, the ribbon is attached to the presynaptic membrane, and postsynaptic horizontal and bipolar cell processes terminate adjacent to the ribbon. Presynaptically, VGLUT1 and, postsynaptically, mGluR6 are expressed. mGluR6 on dendrites of ON bipolar cells is essential for photoreceptor to ON bipolar cell synaptic transmission (Nomura et al., 1994; Masu et al., 1995). Physiologically, ERG recordings from *Bsn* mutant mice still display a small b-wave, demonstrating residual photoreceptor to bipolar cell synaptic transmission. The b-wave in mutant mice is most likely generated by the ribbon synapses in the ONL and the OPL, which escaped the *Bsn* deficiency. The ERG recordings also show that the remaining b-wave is rod driven, corroborating the result that anchored ribbons are found only at rod synapses.

Established animal models of retinal degeneration, showing loss of photoreceptors, are the RCS rat (Bok and Hall, 1971) and the *rd* mouse (Bowes et al., 1990). Studies on retinae of these species showed that with the loss of the photoreceptors, expression of mGluR6 in the postsynaptic rod bipolar cells changed from a punctate dendritic to a diffuse somatic labeling (Nomura et al., 1994; Strettoi and Pignatelli, 2000). In the adult *Bsn* mutant retina, mGluR6 had a punctate expression pattern in rod bipolar cell dendrites, suggesting glutamate release at the remaining ribbon synapses in the OPL and the ONL.

In the retina of a transgenic swine with photoreceptor degeneration, most of the bipolar and horizontal cell processes retract from the presynaptic photoreceptor terminals. But some of the rod bipolar cell dendrites grow out and contact the terminals of surviving cone photoreceptors to form ectopic synapses (Peng et al., 2000). A partial retraction of postsynaptic processes at photoreceptor terminals is also observed in the *Bsn* mutant retina. But strikingly different from the animal models of retinal degenerations is the finding that rod bipolar and horizontal cell processes arborize in the ONL, where they form ectopic ribbon synapses with rod photoreceptors. We have no evidence for rod bipolar cell dendrites contacting cone terminals (O.D. and J.H.B., unpublished data).

We do not know why certain ribbon synapses are immune to *Bsn* deficiency and what molecular mechanisms mediate the genesis of ectopic synapses. Timing might be an important factor, as rod photoreceptors differentiate later in retinal neurogenesis then cone photoreceptors (Marquardt and Gruss, 2002). Undoubtedly, however, Bassoon is a key protein for the formation of the photoreceptor ribbon synapse.

Experimental Procedures

All animal experiments were performed in compliance with the guidelines for the welfare of experimental animals issued by the Federal Government of Germany, the NIH, and the Max Planck Society.

Antibodies

The following anti-Bassoon antibodies were used in this study: a mouse anti-Bassoon mab Sap7f (diluted 1:8000) generated against aa 756–1001 of the Bassoon protein (tom Dieck et al., 1998), and a rabbit anti-Bassoon pab BSN6.3 (diluted 1:3000) generated against aa 95–210 of the Bassoon protein (Altrock et al., 2003). In addition, the following antibodies known to label distinct populations of retinal neurons, synaptic ribbons, or glutamatergic synapses were used: mouse anti-PKCα mab (1:100; Seikagaku, Tokyo, Japan), rabbit anti-PKCα pab (1:10,000; Sigma, Saint Louis, MO), mouse anti-Calbindin mab (1:1000; Sigma), rabbit anti-Calbindin pab (1:2000; Swant, Bellinzona, Switzerland), rabbit anti-Neurokinin-3 pab (1:200; Novus Biologicals, Littleton, CO), mouse anti-Goα mab (1:500; Chemicon, Temecula, VA), mouse anti-Kinesin II mab (1:40; BAbCO, Richmond, CA), rabbit anti-mGluR6 pab (1:1000; Neuromics, Minneapolis, MN), and rabbit anti-vesicular glutamate transporter pab (VGLUT1; 1:10,000; Synaptic Systems, Göttingen, Germany).

Retinal Tissue Preparation and Light and Electron Microscopic Immunocytochemistry

The animals were anesthetized deeply with halothane and decapitated. A description of the preparation of the retinal tissue for light and electron microscopic immunocytochemistry is given in Dick et al. (2001). Briefly, for light microscopy, the eyes were opened and immersion fixed in 4% (w/v) paraform aldehyde (PFA) in phosphate buffer (PB; 0.1 M, pH 7.4) for 15–30 min. For preembedding immunoelectron microscopy, the fixation was in 0.05% glutaraldehyde (GA) and 4% (w/v) PFA in PB for 15 min followed by an additional 35 min in 4% (w/v) PFA in PB. For conventional electron microscopy and good tissue preservation, the fixation was in 2.5% GA and 3% PFA in PB for 2 hr at room temperature followed by an incubation in 2% osmiumtetroxide for 2 hr at 4°C.

For light microscopical analysis, the immunocytochemical labeling was performed by the indirect fluorescence method (Dick et al., 2001). The retinal sections were incubated in the primary antibodies overnight at room temperature. The binding sites of the primary antisera were revealed by secondary antisera, goat anti-rabbit, or goat anti mouse IgG coupled to Alexa 594 (red fluorescence) or Alexa 488 (green fluorescence) (diluted 1:500; Molecular Probes, Eugene, OR). In control experiments, either the primary or secondary antiserum was omitted, resulting in a complete loss of specific immunoreactivity. Single-labeled sections were examined and photographed with a Zeiss photomicroscope (Axiophot; Zeiss, Oberkochen, Germany). Micrographs were taken with a cooled CCD camera (Spot 2; Diagnostic Instruments, Burroughs, MI) in combination with the software program Metaview Software (Universal Imaging, West Chester, PA). For light microscopic analysis of double-labeling experiments, sections were examined with a Zeiss confocal laser scanning microscope equipped with an argon laser and a HeNe laser (LSM5 Pascal; Zeiss, Oberkochen, Germany). To show the branching patterns of horizontal and bipolar cell processes in the outer nuclear layer, stacks of confocal images, spanning from 3 to 12 μm, were collapsed into a single plane. The images were adjusted for contrast and brightness using Adobe Photoshop 5.5, and the figures were arranged using Corel Draw 9.

For electron microscopical analysis, detection of Bassoon immunoreactivity was carried out as detailed previously (Dick et al., 2001). The primary antiserum (BSN6.3) was used at the same concentration and diluted in the same medium, but without Triton X-100, as used for light microscopy. Tissue sections were incubated in primary antiserum for 4 days at 4°C. Binding sites of the primary antiserum were visualized with a biotinylated goat anti-rabbit IgG secondary antiserum diluted 1:100 (Vector Laboratories, Burlinggame, CA) and a peroxidase-based enzymatic detection system (Vectastain Elite ABC kit; Vector Laboratories). The reaction product was silver intensified and gold toned. Controls were carried out as described for

the light microscopic immunocytochemistry. Ultrathin sections were examined and photographed with a Zeiss EM10 electron microscope (Zeiss, Oberkochen) and a GATAN BioScan digital camera (1.024 × 1.024 pixel; GATAN, Munich, Germany) in combination with the software program DIGITAL MICROGRAPH 3.1 (GATAN, Pleasanton, CA).

Quantitative Analysis

To quantify the morphological phenotype of rod photoreceptor ribbon synapses, we examined two wt and two homozygous *Bsn* mutant mice from the same litter for each of the developmental stages and in the adult. For each stage, we photographed 150 images at a magnification of 20,000× using single ultrathin sections (a single image contained about four photoreceptor terminals). To ensure that the counts were unbiased, the observer was blind to the condition as to whether the images were taken from wt or *Bsn* mutant retinae.

For the adult stage, the number of the examined terminals was counted, and the terminals were subdivided into different groups depending on their ultrastructural appearance: (1) terminals containing a ribbon triadic complex with the ribbon attached to the synaptic site, (2) terminals containing only a free-floating ribbon, (3) terminals containing postsynaptic elements and a free-floating ribbon, (4) terminals containing only postsynaptic elements, and (5) empty terminals. For the developmental study, we proceeded as described above, but we kept the subdivision into the different groups more simple: (1) terminals containing a ribbon triadic complex with the ribbon attached to the synaptic site, (2) terminals containing a free floating ribbon, and (3) empty terminals.

Electroretinogram (ERG) Measurements

Before an experimental session, animals were dark adapted for at least 12 hr. Mice (8–14 weeks old) were anaesthetized by intraperitoneal injections of xylazine (50 mg/kg) and ketamine (20 mg/kg), and the pupils were dilated with 1% atropine sulfate. Surgery and subsequent handling were done under dim, red dark-room light. A continuously moistened Ag/AgCl cotton-wick electrode was placed on the corneal surface, and a needle reference electrode was inserted subcutaneously into the skin covering the skull. A needle grounding electrode was inserted into the tail. The mouse was laid on its side with the head fixed with surgical tape. Electrical potentials were recorded and bandpass filtered (1–1000 Hz) using a DAM50 Bioamplifier (WPI, Sarasota, FL). Online averaging and storage was done with the MacLab system (AD Instruments, Hastings, UK) connected to an Apple PowerPC. Full field test and background lights were generated with two 150 W halogen light sources and focused onto the cornea. Intensities were adjusted with neutral-density filters, and test flash duration was controlled with an electromagnetic shutter. Corneal illuminance for white light (lx) was measured with a calibrated luxmeter (Palux; Gossen GmbH, Nürnberg, Germany) at the position of the cornea.

Two different experimental paradigms were chosen for ERG measurements: scotopic intensity-response curves were measured with 20 ms white light flashes and a stimulus interval of 10 s. These relatively short stimulus intervals had to be chosen in order to be able to finish the measurements, because after some time *Bsn* mutant mice developed seizures which made further recording impossible. Therefore, the retina was probably not fully dark adapted when high-intensity stimuli were used. At each intensity 16–32 responses were averaged. For analysis, response amplitudes were measured relative to the baseline, which was determined by the mean voltage within a 100 ms period before the light flash. Implicit time (time-to-peak) was determined as the temporal difference between light onset and the time when maximum response was reached. For the incremental threshold functions, steady white background lights with increasing corneal illuminance were applied by the second beam. Each background was given for 5 min before white light test flashes (20 ms duration, 0.75 s interval, 16–32 responses averaged) of increasing illuminance were superimposed. The threshold illuminance was determined by fitting a Michaelis-Menten function through the response amplitude data for each background intensity. A 20μV criterion response was chosen as threshold, and the illuminance required to produce the threshold was interpolated from the fitting curves (Green et al., 1991). Data from a total of six *Bsn* mutant mice and eight corresponding wt littermates were included in the ERG analysis.

Acknowledgments

We are grateful to Anja Hildebrand, Gong-Sun Nam, and Walter Hofer for expert technical assistance, and to Dr. Keely Bumsted O'Brien for critically reading the manuscript. This work was supported by the Deutsche Forschungsgemeinschaft SFB269/B4 (J.H.B.), SFB 426 (E.D.G.), Fonds der Chemischen Industrie (E.D.G.), National Institute of Health P50 HD32901, NIH RO1 NS39471, PO1 AG06569 (C.C.G.), and a Heisenberg Fellowship to J.H.B.

Received: September 11, 2002
Revised: December 9, 2002

References

Allwardt, B.A., Lall, A.B., Brockerhoff, S.E., and Dowling, J.E. (2001). Synapse formation is arrested in retinal photoreceptors of the zebrafish *nrc* mutant. J. Neurosci. *21*, 2330–2342.

Altrock, W.D., tom Dieck, S., Sokolov. M., Meyer, A.C., Sigler, A., Brakebush, C., Fässler, R., Richter, K., Boeckers, T.M., Potschka, H., et al. (2003). Functional inactivation of a fraction of excitatory synapses in mice deficient for the active zone protein Bassoon. Neuron *37*, this issue, 787–800.

Blanks, J.C., Adinolfi, A.M., and Lolley, R.N. (1974). Synaptogenesis in the photoreceptor terminal of the mouse retina. J. Comp. Neurol. *156*, 81–94.

Bok, D., and Hall, M.O. (1971). The role of the pigment epithelium in the etiology of inherited retinal dystrophy in the rat. J. Cell Biol. *49*, 664–682.

Bowes, C., Li, T., Dancer, M., Baxter, L.C., Applebury, M.L., and Farber, D. (1990). Retinal degeneration in the *rd* mouse is caused by a defect in the β subunit of rod cGMP-phosphodiesterase. Nature *347*, 677–680.

Boycott, B.B., and Wässle, H. (1999). Parallel processing in the mammalian retina. Invest. Ophthalmol. Vis. Sci. *40*, 1313–1327.

Brandstätter, J.H., and Hack, I. (2001). Localization of glutamate receptors at a complex synapse. The mammalian photoreceptor synapse. Cell Tissue Res. *303*, 1–14.

Brandstätter, J.H., Fletcher, E.L., Garner, C.C., Gundelfinger, E.D., and Wassle, H. (1999). Differential expression of the presynaptic cytomatrix protein Bassoon among ribbon synapses in the mammalian retina. Eur. J. Neurosci. *11*, 3683–3693.

Cases-Langhoff, C., Voss, B., Garner, A.M., Appeltauer, U., Takei, K., Kindler, S., Veh, R.W., De Camilli, P., Gundelfinger, E.D., and Garner, C.C. (1996). Piccolo, a novel 420 kDa protein associated with the presynaptic cytomatrix. Eur. J. Cell Biol. *69*, 214–223.

Casini, G., Brecha, N.C., Bosco, L., and Rickman, D.W. (2000). Developmental expression of neurokinin-1 and neurokinin-3 receptors in the rat retina. J. Comp. Neurol. *421*, 275–287.

DeVries, S.H., and Baylor, D.A. (1993). Synaptic circuitry of the retina and olfactory bulb. Cell Suppl., *72*, 139–149.

Dick, O., Hack, I., Altrock, W.D., Garner, C.C., Gundelfinger, E.D., and Brandstätter, J.H. (2001). Localization of the presynaptic cytomatrix protein Piccolo at ribbon and conventional synapses in the rat retina: comparison with Bassoon. J. Comp. Neurol. *439*, 224–234.

Dowling, J.E. (1987). The Retina: An Approachable Part of the Brain. (Cambridge, MA: Harvard University Press).

Dresbach, T., Qualmann, B., Kessels, M.M., Garner, C.C., and Gundelfinger, E.D. (2001). The presynaptic cytomatrix of brain synapses. Cell. Mol. Life Sci. *58*, 94–116.

Fenster, S.D., Chung, W.J., Zhai, R., Cases-Langhoff, C., Voss, B., Garner, A.M., Kampf, U., Kindler, S., Gundelfinger, E.D., and Garner, C.C. (2000). Piccolo, a presynaptic zinc finger protein structurally related to Bassoon. Neuron *25*, 203–214.

Garner, C.C., Kindler, S., and Gundelfinger, E.D. (2000). Molecular determinants of presynaptic active zones. Curr. Opin. Neurobiol. *10*, 321–327.

Green, D.G., Herreros, D.T., and Glover, M.J. (1991). Are albino rats night blind? Invest. Ophthalmol. Vis. Sci. *32*, 2366–2371.

Haverkamp, S., and Wässle, H. (2000). Immunocytochemical analysis of the mouse retina. J. Comp. Neurol. *424*, 1–23.

Hermes, B., Reuss, S., and Vollrath, L. (1992). Synaptic ribbons, spheres and intermediate structures in the developing rat retina. Int. J. Dev. Neurosci. *10*, 215–223.

Kolb, H., and Nelson, R. (1995). The organization of photoreceptor to bipolar synapses in the outer plexiform layer. In Neurobiology and Clinical Aspects of the Outer Retina, M.B.A. Djamgoz, S.N. Archer, and S. Vallerga eds. (London: Chapman and Hall), pp. 273–296.

Lenzi, D., and von Gersdorff, H. (2001). Structure suggests function: the case for synaptic ribbons as exocytotic nanomachines. Bioessays *23*, 831–840.

Libby, R.T., Lavallee, C.R., Balkema, G.W., Brunken, W.J., and Hunter, D.D. (1999). Disruption of laminin β2 chain production causes alterations in morphology and function in the CNS. J. Neurosci. *19*, 9399–9411.

Marquardt, T., and Gruss, P. (2002). Generating neuronal diversity in the retina: one for nearly all. Trends Neurosci. *25*, 32–38.

Masu, M., Iwakabe, H., Tagawa, Y., Miyoshi, T., Yamashita, M., Fukuda, Y., Sasaki, H., Hiroi, K., Nakamura, Y., Shigemoto, R., et al. (1995). Specific deficit of the ON response in visual transmission by targeted disruption of the mGluR6 gene. Cell *80*, 757–765.

Muresan, V., Lyass, A., and Schnapp, B.J. (1999). The kinesin motor KIF3A is a component of the presynaptic ribbon in vertebrate photoreceptors. J. Neurosci. *19*, 1027–1037.

Nomura, A., Shigemoto, R., Nakamura, Y., Okamoto, N., Mizuno, N., and Nakanishi, S. (1994). Developmentally regulated postsynaptic localization of a metabotropic glutamate receptor in rat rod bipolar cells. Cell *77*, 361–369.

Peichl, L., and González-Soriano, J. (1994). Morphological types of horizontal cell in rodent retinae: a comparison of rat, mouse, gerbil, and guinea pig. Vis. Neurosci. *11*, 501–517.

Peng, Y.-W., Hao, Y., Petters, R.M., and Wong, F. (2000). Ectopic synaptogenesis in the mammalian retina caused by rod photoreceptor-specific mutations. Nat. Neurosci. *3*, 1121–1127.

Rao-Mirotznik, R., Harkins, A.B., Buchsbaum, G., and Sterling, P. (1995). Mammalian rod terminal: architecture of a binary synapse. Neuron *14*, 561–569.

Richter, K., Langnaese, K., Kreutz, M.R., Olias, G., Zhai, R., Scheich, H., Garner, C.C., and Gundelfinger, E.D. (1999). Presynaptic cytomatrix protein Bassoon is localized at both excitatory and inhibitory synapses of rat brain. J. Comp. Neurol. *408*, 437–448.

Rieke, F., and Schwartz, E.A. (1996). Asynchronous transmitter release: control of exocytosis and endocytosis at the salamander rod synapse. J. Physiol. (London) *493*, 1–8.

Ruether, K.R., Grosse, J., Matthiessen, E., Hoffmann, K., and Hartmann, C. (2000). Abnormalities of the photoreceptor-bipolar cell synapse in a substrain of C57BL/10 mice. Invest. Ophthalmol. Vis. Sci. *41*, 4039–4047.

Schmitz, F., Königstorfer, A., and Südhof, T.C. (2000). RIBEYE, a component of synaptic ribbons: a protein's journey through evolution provides insight into synaptic ribbon function. Neuron *28*, 857–872.

Steinberg, R.H., Frishman, L.J., and Sieving, P.A. (1991). Negative components of the electroretinogram from proximal retina and photoreceptor. In Progress in Retinal Research, N.N. Osborne and G.J. Chader, eds. (Oxford: Pergamon), pp. 121–160.

Strettoi, E., and Pignatelli, V. (2000). Modifications of retinal neurons in a mouse model of retinitis pigmentosa. Proc. Natl. Acad. Sci. USA *97*, 11020–11025.

Takamori, S., Rhee, J.S., Rosenmund, C., and Jahn, R. (2000). Identification of a vesicular glutamate transporter that defines a glutamatergic phenotype in neurons. Nature *407*, 189–194.

tom Dieck, S., Sanmarti-Vila, L., Langnaese, K., Richter, K., Kindler, S., Soyke, A., Wex, H., Smalla, K.-H., Kampf, U., Franzer, J.T., et al. (1998). Bassoon, a novel zinc-finger CAG/glutamine-repeat protein selectively localized at the active zone of presynaptic nerve terminals. J. Cell Biol. *142*, 499–509.

Vardinon-Friedman, H., Bresler, T., Garner, C.C., and Ziv, N.E. (2000). Assembly of new individual excitatory synapses: time course and temporal order of synaptic molecule recruitment. Neuron *27*, 57–69.

Vollrath, L., and Spiwoks-Becker, I. (1996). Plasticity of retinal ribbon synapses. Microsc. Res. Tech. *35*, 472–487.

von Gersdorff, H. (2001). Synaptic ribbons: versatile signal transducers. Neuron *29*, 7–10.

Wang, X., Kibschull, M., Laue, M.M., Lichte, B., Petrasch-Parwez, E., and Kilimann, M.W. (1999). Aczonin, a 550-kD putative scaffolding protein of presynaptic active zones, shares homology regions with Rim and Bassoon and binds profilin. J. Cell Biol. *147*, 151–162.

Zhai, R.G., Vardinon-Friedman, H., Cases-Langhoff, C., Becker, B., Gundelfinger, E.D., Ziv, N.E., and Garner, C.C. (2001). Assembling the presynaptic active zone: a characterization of an active zone precursor vesicle. Neuron *29*, 131–143.